Nov 5th -

Cold-Formed Steel Channel Sections with Web Stiffeners Subjected to Local and Distortional Buckling — Part I: Tests and Finite Element Analysis

Liping Wang

Ben Young

Twenty-Second International Specialty Conference on Cold-Formed Steel Structures
St. Louis, Missouri, USA, November 5 & 6, 2014

Cold-formed Steel Channel Sections with Web Stiffeners subjected to Local and Distortional Buckling — Part I: Tests and Finite Element Analysis

Liping Wang[1] and Ben Young[2]

Abstract

An experimental investigation of simply supported beams with two different stiffened channel sections has been conducted under both four-point bending and three-point bending about the major axis of the sections. Stiffeners were employed to the web of plain channel and lipped channel sections to improve the flexural strength of cold-formed steel sections that are prone to local buckling and distortional buckling. In this study, the channel sections were brake-pressed from high strength zinc-coated grades G500 and G550 structural steel sheets with nominal 0.2% proof stresses of 500 and 550 MPa, respectively. The high strength stiffened channel sections had the thicknesses of 0.48, 1.0 and 1.2 mm. Material properties were obtained from the tensile coupon tests. The moment capacities and observed failure modes at ultimate loads in the beam tests were reported. A nonlinear finite element model (FEM) was developed and verified against the test results in terms of strengths, failure modes and moment-curvature curves. It is shown that the FEM well predicted the moment capacities and failure modes of the test beams.

Introduction

Cold-formed steel sections are usually manufactured into channel sections, Z-sections, hat sections and some other open sections by cold-rolling or brake-pressing technique. The plate elements constituting the cold-formed steel

[1] PhD student, Department of Civil Engineering, The University of Hong Kong, Pokfulam Road, Hong Kong, China
[2] Professor, Department of Civil Engineering, The University of Hong Kong, Pokfulam Road, Hong Kong, China

sections usually have large width-to-thickness ratio. Hence, local buckling and distortional buckling are usually the governing failure modes for cold-formed steel members.

Extensive investigations have been conducted on cold-formed steel conventional sections and design rules can be found in the specifications of different countries, such as the European Code (EC3, 2006), North American Specification (NAS, 2012) and Australian/New Zealand Standard (AS/NZS, 2005). In recent years, efforts have been made by some researchers to investigate the structural behaviour of cold-formed steel stiffened sections. These studies include the channel columns with inclined lips (Young & Hancock, 2003; Zhang et al., 2007), channel columns with returned lip stiffeners (Young & Yan, 2004), concentrically loaded compression members with equal lipped angles (Young, 2005), columns with non-symmetric lipped angle sections (Young & Chen, 2008a), columns of built-up closed and open sections with intermediate stiffeners (Young & Chen, 2008b; Zhang & Young, 2012), and beams with both edge and intermediate stiffeners in the compression flanges of Z-sections (Haidarali & Nethercot, 2012).

However, it was found that limited investigation have been conducted on cold-formed steel stiffened sections subjected to bending. Therefore, this study focused cold-formed steel beams with stiffened channel sections subjected to local buckling and distortional buckling. A total of 13 simply supported beams were tested under both four-point bending and three-point bending about the major axis of the sections. The moment capacities and corresponding failure modes were obtained. In addition, a nonlinear finite element model was developed for stiffened channel sections subjected to four-point bending. The finite element model was verified against the four-point bending tests conducted in this study.

Experimental Investigation

Test Specimens

A total of 26 cold-formed steel specimens of single channels with complex intermediate and edge stiffeners were tested subjected to bending about the major *x*-axis. Two identical stiffened channels were tested at the same time in order to avoid out-of-plane bending. Therefore, a total of 13 beam tests was conducted. In this study, two section shapes were investigated including the plain channel section with web stiffener (PWS-section) and lipped channel section with web stiffener (LWS-section) as shown in Fig. 1. The channel

sections were brake-pressed from high strength zinc-coated grades G500 and G550 structural steel sheets with nominal 0.2% proof stresses of 500 and 550 MPa, respectively. Two plate thicknesses of 0.48 and 1.0 mm were tested for PWS-section, while an additional plate thickness of 1.2 mm was tested for LWS-section. The angle of inclined web element (θ) was 45^o, and 60^o from the vertical axis for PWS-sections, and LWS-sections, respectively. The cross-section dimensions of all specimens were measured and reported in Tables 1 – 2.

The test specimens were cut into a specified length of 1400 mm for all the channels. The beam specimens were selected to have a relatively short span, which was aimed to investigate the local buckling and distortional buckling of the stiffened sections.

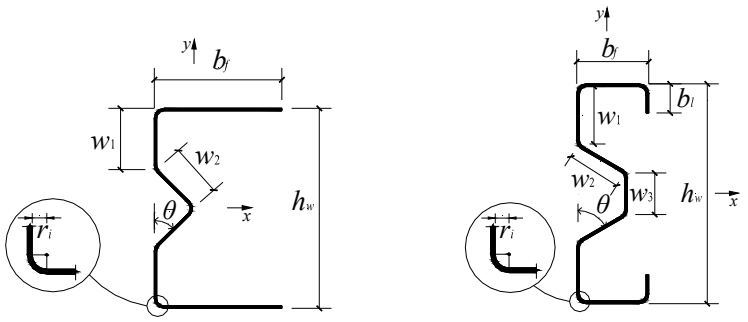

(a) PWS-section (b) LWS-section

Figure 1: Definition of symbols

Specimen Labelling

The test specimens were labelled with characteristic information such that each beam can be easily identified, as illustrated in Fig. 2. For example, the label "PWS-0.48-B4R-a", where "PWS" refers to the PWS-sections as shown in Fig. 1(a), "0.48" indicates that the plate thickness is 0.48 mm, and "B4" refers to the four-point bending test about the major axis. If a test was repeated, then a symbol of "R" was added after “B4”. Finally, "a" indicates the channel "a" of a pair of channels tested at the same time.

Tensile Coupon Tests

The material properties of the test specimens were obtained by carrying out tensile coupon tests. The coupon specimens were prepared in accordance with the Australian standard AS 1391 (Australian Standard, 2007). The flat tensile

coupons were extracted in the longitudinal direction of the beam test specimens. Two coupon specimens were tested for each of the five different sections. The material properties including initial Young's modulus (E), 0.2% proof stress ($\sigma_{0.2}$), tensile ultimate strength (σ_u), and strain at fracture (ε_f) based on the gauge length of 50mm of the coupon specimens were obtained and summarized in Table 3.

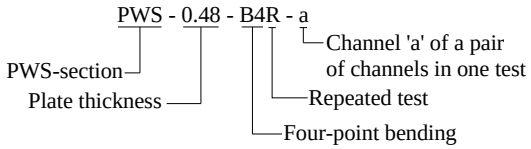

Figure 2: Label of test specimens

An MTS testing machine with loading capacity of 50 kN was used to test the tensile coupons. The gauge length of coupon specimens was 50 mm, and a calibrated extensometer of 50 mm was used to measure the longitudinal strain during the tests. Two linear strain gauges were also attached at the center of two surfaces of each coupon, and the initial strain readings were used to determine the Young's modulus. Displacement control was used and tension load was applied to the coupon specimens with the loading rate of 0.05 mm/min from the beginning to approximately 100 MPa in the coupon specimens, and then the loading rate was changed to 0.2 mm/min until the 0.2% proof stress has reached. The loading rate was then changed to 0.6 mm/min until the coupon specimen failed. In order to eliminate the influence of different loading rates on the test results, all coupon tests were paused for 90 seconds at three different locations of the stress-strain curves. The locations were near the 0.2% proof stress, near the ultimate strength and just before the fracture of the coupon specimen. The static stress-strain curves can then be obtained accordingly. The material properties based on the static stress-strain curves are shown in Table 3.

Test Rig and Operation

The schematic views of four-point bending and three-point bending test arrangements are shown in Fig. 3 and Fig. 4, respectively. The beams were simply supported. The hinge support was simulated by half round, which allows only in-plane rotation. The roller support was simulated by round bar, which allows both in-plane rotation and translation movement along the specimen. Two channels were tested at the same time that bolted to T-shaped aluminum blocks, as shown in Fig. 5. These aluminum blocks were located at the loading

points and end supports. The sectional views at the loading points and end supports of the T-shaped aluminum blocks for the three different sections are detailed in Fig. 5. A servo-controlled hydraulic testing machine was used to apply a downward force to the spreader beam. The static load was recorded by pausing for 90 seconds near the ultimate load. This allowed the stress relaxation associated with plastic straining to take place. A data acquisition system was used to record the displacement transducers and load readings at regular intervals during the tests.

Specimens	Flange	Web			Thickness		Radius
	b_f	h_w	w_1	w_2	t	t^*	r_i
	(mm)	(mm)	(mm)	(mm)	(mm)	(mm)	(mm)
PWS-0.48-B4-a	54.1	85.4	25.2	23.0	0.551	0.461	3.9
PWS-0.48-B4-b	53.9	85.5	25.6	23.5	0.557	0.467	3.5
PWS-0.48-B4R-a	53.0	87.0	26.5	23.0	0.560	0.470	3.5
PWS-0.48-B4R-b	53.7	87.1	26.1	23.4	0.562	0.472	3.6
PWS-0.48-B3-a	54.0	85.4	26.1	22.1	0.565	0.475	3.6
PWS-0.48-B3-b	53.9	85.9	25.8	24.8	0.557	0.467	3.6
PWS-1.0-B4-a	54.4	85.0	25.7	23.4	1.041	1.003	3.1
PWS-1.0-B4-b	54.0	85.1	26.3	23.0	1.050	1.012	3.1
PWS-1.0-B4R-a	54.6	86.2	26.9	22.7	1.043	1.005	3.3
PWS-1.0-B4R-b	53.6	86.1	26.8	22.3	1.046	1.008	3.5
PWS-1.0-B3-a	55.0	85.7	27.1	22.6	1.047	1.009	3.3
PWS-1.0-B3-b	54.0	86.2	26.6	23.0	1.052	1.014	3.4

t^* is the base metal thickness

Table 1: Measured dimensions of PWS-section test specimens

Four-point bending tests

The four-point bending tests were loaded symmetrically at two points to the T-shaped aluminum blocks through a spreader beam, as shown in Fig. 3. Half round and round bar were also used at the two loading points. In this testing arrangement, pure in-plane bending of the specimens can be obtained between the two loading points without the presence of shear and axial forces. The distance between the two loading points was 600 mm for all four-point bending test beams. This distance was selected such that the ultimate load causing failure in the moment span is lower than that causing failure in the shear span. Displacement control was adopted to drive the hydraulic actuator at a constant rate of 0.3 mm/min for the four-point bending tests. Four displacement transducers (LVDTs 1 - 4) were positioned at the end supports to measure the end rotation of the beams. Three transducers (LVDTs 5 - 7) were positioned at the tension flange near the flange-web junctions to measure the vertical

deflection and curvature of the beams. One transducer (LVDT 8) was positioned near the free edge of compression flange at mid-span to monitor the possible local buckling or distortional buckling. Two strain gauges were also adhered to the middle and near the flange-web junction of the compression flange at mid-span for some of the LWS-section specimens in order to monitor the possible local buckling.

Specimens	Lip	Flange	Web				Thickness		Radius
	b_l (mm)	b_f (mm)	h_w (mm)	w_1 (mm)	w_2 (mm)	w_3 (mm)	t (mm)	t^* (mm)	r_i (mm)
LWS-0.48-B4-a	12.6	32.0	99.7	26.1	26.1	18.0	0.556	0.464	3.8
LWS-0.48-B4-b	12.6	32.2	99.3	25.9	25.4	18.1	0.545	0.453	3.8
LWS-0.48-B3-a	12.4	32.3	98.5	26.2	25.1	18.6	0.554	0.462	3.8
LWS-0.48-B3-b	12.8	32.4	99.2	26.5	25.8	18.4	0.557	0.465	3.8
LWS-1.0-B4-a	13.6	32.5	98.0	26.9	25.7	18.3	1.064	1.022	3.4
LWS-1.0-B4-b	13.5	32.7	97.6	26.5	26.3	17.7	1.062	1.020	3.1
LWS-1.0-B3-a	13.1	32.4	98.1	26.7	25.9	17.9	1.036	0.994	3.3
LWS-1.0-B3-b	13.3	32.3	98.4	27.0	26.2	17.7	1.042	1.000	3.3
LWS-1.0-B3R-a	13.6	32.5	97.6	26.3	26.2	17.9	1.054	1.012	3.5
LWS-1.0-B3R-b	13.5	32.6	98.4	27.0	25.6	18.7	1.053	1.011	3.5
LWS-1.2-B4-a	12.6	32.5	100.4	26.2	26.7	19.1	1.257	1.221	3.4
LWS-1.2-B4-b	13.3	32.3	100.6	26.5	26.9	18.2	1.245	1.209	3.3
LWS-1.2-B3-a	13.3	32.3	100.3	26.5	26.8	18.7	1.244	1.208	3.5
LWS-1.2-B3-b	13.2	32.5	100.0	26.1	27.3	18.3	1.246	1.210	3.3

t^* is the base metal thickness

Table 2: Measured dimensions of LWS-section test specimens

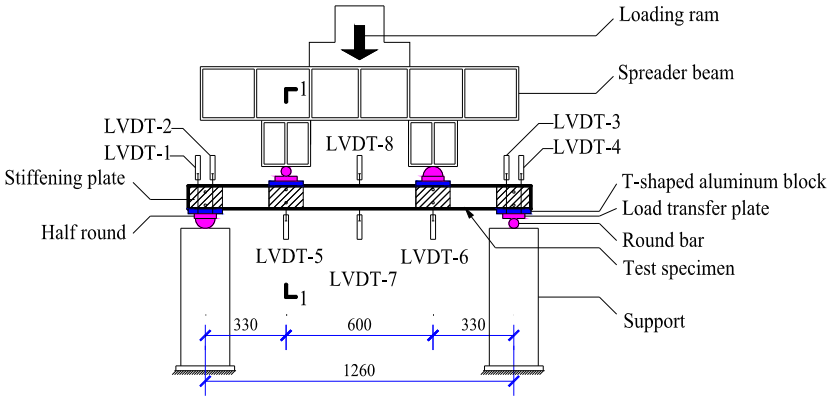

Figure 3: Schematic view of four-point bending test arrangement

Three-point bending tests

The three-point bending tests were loaded at the mid-span to the T-shaped aluminum blocks using a round bar, as shown in Fig. 4. The spans between the loading point and the supports were 630 mm for all three-point bending tests. Displacement control was adopted to drive the hydraulic actuator at a constant rate of 0.5 mm/min, which is a faster loading rate compared to the four-point bending tests. However, the static load was obtained by pausing the hydraulic actuator for 90 seconds near the ultimate load. Therefore, the effect of different loading rate was eliminated. One transducer was positioned on the tension flange near the flange-web junction at the mid-span of specimens to measure the vertical deflection of the beams. Two transducers were positioned at the end of the specimens with half round to measure the end rotation of the beams.

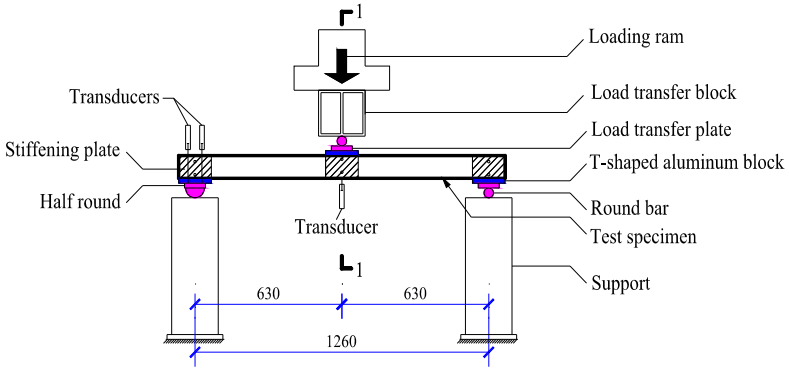

Figure 4: Schematic view of three-point bending test arrangement

Coupon specimens	Nominal	Measured results			
	$\sigma_{0.2}$ (MPa)	E (GPa)	$\sigma_{0.2}$ (MPa)	σ_u (MPa)	ε_f (%)
PWS-0.48	550	213	682	728	1.6
PWS-0.48R		213	661	690	2.0
LWS-0.48	550	216	689	744	1.5
LWS-0.48R		213	661	705	2.0
PWS-1.0	500	215	604	606	8.7
PWS-1.0R		213	598	599	9.7
LWS-1.0	500	216	599	600	10.0
LWS-1.0R		216	592	599	8.6
LWS-1.2	500	212	603	611	8.8
LWS-1.2R		210	603	610	9.2

Table 3: Material properties obtained from tensile coupon tests

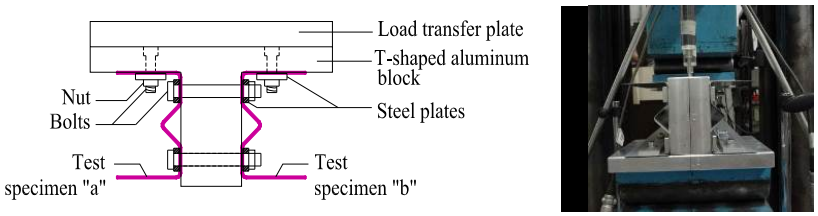

Section 1-1 End view

(a) PWS-sections

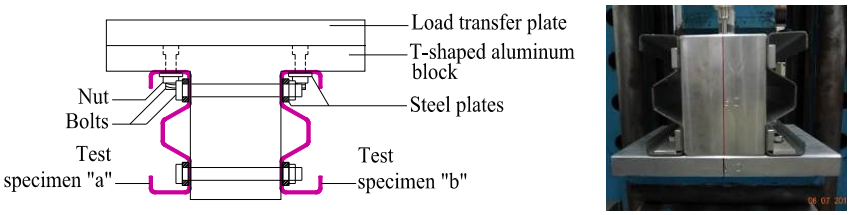

Section 1-1 End view

(b) LWS-sections

Figure 5: Details of the T-shaped aluminum load transfer blocks at loading points and end supports

Test Results

The specimens failed in the moment span for all the four-point bending tests, and failed near the loading point for all the three-point bending tests. Out-of-plane bending of the specimens was not observed in the tests. The experimental ultimate moments per channel were obtained using a quarter of the ultimate static applied load multiplied by the lever arm (distance from the end support to the loading point) for the beam specimens. The weight of the T-shaped aluminum blocks, half rounds, round bars and other steel plates were also included in the calculation of the ultimate moments. Local buckling (Fig. 6(a)), distortional buckling (Fig. 6(b)) and their interaction with global flexural buckling were observed in the beam tests. The failure mode was defined at the moment when the ultimate load reached.

The ultimate moments per channel of the beams subjected to four-point bending ($M_{EXP\text{-}4p}$) were compared to those subjected to three-point bending ($M_{EXP\text{-}3p}$), as shown in Table 4. It was found that the ultimate moments of the specimens subjected to three-point bending are on average 11% higher than those specimens subjected to four-point bending, and the maximum value of $M_{EXP\text{-}3p}$ / $M_{EXP\text{-}4p}$ ratio is 21%.

Specimens	M_{EXP-4p} per channel (kNmm)	Failure mode	Specimens	M_{EXP-3p} per channel (kNmm)	Failure mode	$\frac{M_{EXP-3p}}{M_{EXP-4p}}$
PWS-0.48-B4	591	L+F	PWS-0.48-B3	640	L+F	1.08
PWS-1.0-B4	1809	L+F	PWS-1.0-B3	2191	L+F	1.21
LWS-0.48-B4	1029	L+D+F	LWS-0.48-B3	1158	L+D+F	1.13
LWS-1.0-B4	2985	D+F	LWS-1.0-B3	3103	D+F	1.04
LWS-1.2-B4	3807	D+F	LWS-1.2-B3	4235	D+F	1.11
					Mean	1.11

L=Local buckling; D=Distortional buckling; F=Flexural buckling

Table 4: Comparison of test results between three-point bending and four-point bending tests

Finite Element Analysis

The finite element package ABAQUS (2011) was used to develop a finite element model and perform nonlinear analysis of the test beams with stiffened channel sections subjected to four-point bending. Only one channel of the beam was modelled due to symmetry. The measured cross-section dimensions were used in the finite element model. The model was created based on the centerline dimensions of the cross-sections and the base metal thicknesses.

Material Model

The measured material properties obtained from the coupon tests were included in the finite element model using a mathematical model, in which the true stress (σ_{true}) and the logarithmic plastic strain (ε_{pl}) were adopted. The true stress and plastic strain were calculated from the static engineering stress (σ) and strain (ε), which were obtained by the tensile coupon tests. The static stress-strain curve with the lower 0.2% proof stress for the same specimen of each section was used in the finite element analysis. The material properties of the flat potions were also used for the round corners of the sections in the finite element model. This is because a small difference in the numerical results for including the corner material properties compared to those using the flat material properties.

Boundary and Loading Conditions

In the beam tests, the concentrated loads and reaction forces were transferred from the load transfer plates to the T-shaped aluminum blocks and then to the specimens. Therefore, in the finite element model, the interface between the aluminum blocks and the specimen was carefully modelled using coupling constraint, which restrains the motion of a surface to the motion of a single point. A coupling constraint was used at each loading point and support. In each coupling constraint, the contact surfaces between the T-shaped aluminum block and the specimen were defined as a surface set. A reference point was created to represent the loading point or point of reaction force and subsequently defined as a node set. The surface set was then coupled with the corresponding node set in all degrees of freedoms by kinematic method. The loading and boundary conditions were applied to the node sets.

The simply supported boundary condition was modelled by releasing the in-plane rotation at the half round end support (pin support), and releasing both the in-plane rotation and axial displacement along the specimen at the round bar end support (roller support). The vertical load was applied to the node sets at two loading points of the beam using displacement control with a specified displacement value. This value was chosen to be larger than the measured maximum deflection under the loading points in the tests to ensure that the numerical analysis can reach the ultimate load. The static RIKS method was adopted for the load step, in which the nonlinear geometric parameter (*NLGEOM) was used to perform the large displacement analysis.

Element Type and Mesh

The S4R element, a 4-node doubly curved thin or thick shell with reduced integration, hourglass control, and finite membrane strains was used in this study. The finite element mesh size of the beam model was investigated to provide both accurate and time-efficient results. The final mesh size was approximately 5 × 5 mm (length by width) in the flat portions of the cross-sections and a finer mesh at the round corners was used.

Verification of Finite Element Model

The developed finite element model was verified against the experimental results. The moment capacities and failure modes predicted by the finite element analysis (FEA) were compared with the test results, as shown in Table 5. The mean value of the experimental-to-FEA moment capacity (M_{EXP} / M_{FEA}) ratio is 1.03 with the coefficient of variation (COV) of 0.060. The failure modes of local

buckling and distortional buckling obtained from the FEA at ultimate load compared well with the tests, as shown in Fig. 6. The moment-curvature curves of specimen “LWS-0.48-B4” for one channel obtained from the test and FEA are in very good agreement, as shown in Fig. 7. Hence, the finite element model was verified against the tests and showed to be accurate in terms of ultimate moment, failure mode, and moment-curvature curve.

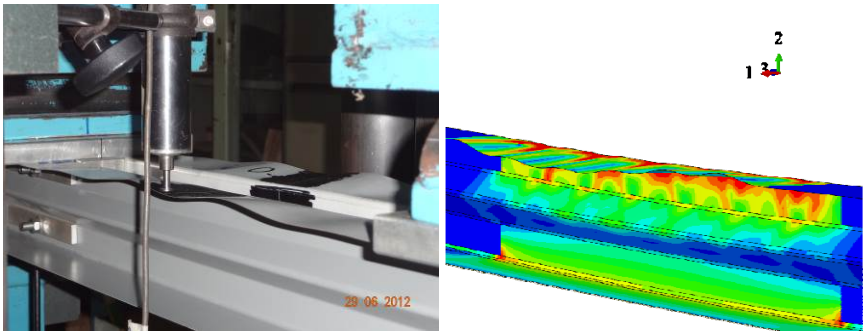

(a) Local buckling

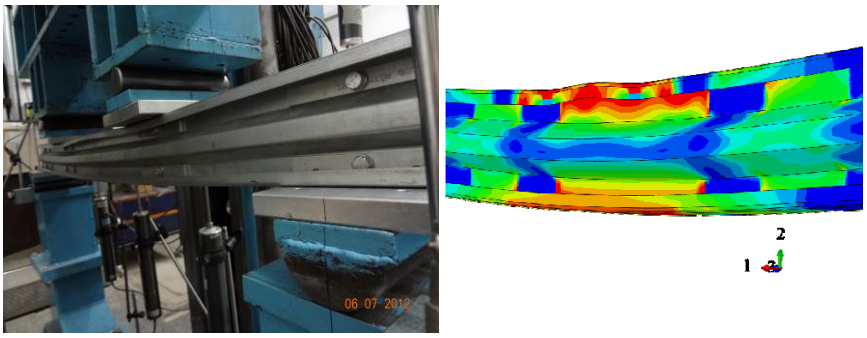

(b) Distortional buckling

Figure 6: Comparison of experimental and numerical failure modes of beam specimens at ultimate load

Specimens	Tests (per channel)		FEA (per channel)		Comparison
	M_{EXP} (kNmm)	Failure mode	M_{FEA} (kNmm)	Failure mode	$\frac{M_{EXP}}{M_{FEA}}$
PWS-0.48-B4	591	L+F	592	L+F	1.00
PWS-0.48-B4R	678	L+F	592	L+F	1.15
PWS-1.0-B4	1809	L+F	1899	L+F	0.95
PWS-1.0-B4R	1929	L+F	1899	L+F	1.02
LWS-0.48-B4	1029	L+D+F	976	L+D+F	1.05
LWS-1.0-B4	2985	D+F	2976	D+F	1.00
LWS-1.2-B4	3807	D+F	3738	D+F	1.02
				Mean	1.03
				COV	0.060

L=Local buckling; D=Distortional buckling; F=Flexural buckling

Table 5: Comparison of moment capacities obtained from FEA results with test results

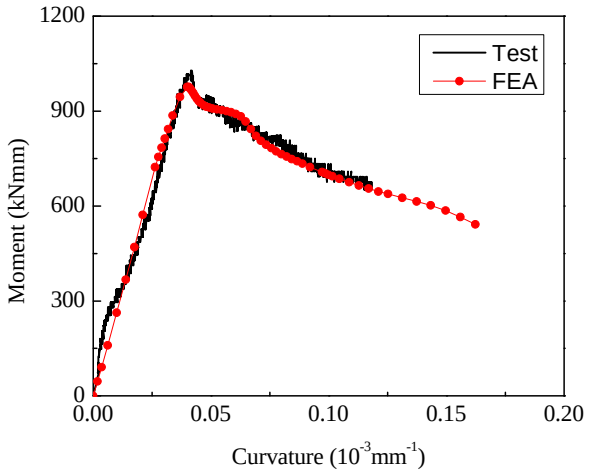

Figure 7: Comparison of moment-curvature curves obtained from test and FEA for one channel specimen LWS-0.48-B4

Conclusions

The experimental and numerical investigation of cold-formed steel channels with stiffened web subjected to bending have been presented. The high strength stiffened channel sections had the measured 0.2% proof stress ranged from 592 to 689 MPa, and the thickness ranged from 0.45 to 1.22mm. Simply supported beams were tested under both four-point bending and three-point bending about the major axis of the sections. The moment capacities and the corresponding failure modes were reported. It was found that the ultimate moments of the specimens subjected to three-point bending are on average 11% higher than those specimens subjected to four-point bending. In addition, a nonlinear finite element model (FEM) was developed and verified against the test results. The FEM closely predicted the behaviour of cold-formed steel channel sections with web stiffeners subjected to local and distortional buckling.

Appendix. – References

ABAQUS. (2011). Dassault Systemes Simulia Corp, *ABAQUS Standard User's Manual*. Version 6.11. USA.

AS/NZS. (2005). *Australian/New Zealand standard-Cold-formed steel structures*. AS/NZS 4600:2005, Standards Australia / Standards New Zealand, Sydney.

Australian Standard. (2007). *Metallic materials—tensile testing at ambient temperature*. AS1391:2007, Standards Australia, Sydney.

EC3. (2006). *Design of steel structures - Part 1-3: General rules – Supplementary rules for cold-formed members and sheeting*. EN 1993-1-3, European Committee for Standardization, Brussels.

Haidarali MR, Nethercot DA. (2012). "Local and distortional buckling of cold-formed steel beams with both edge and intermediate stiffeners in their compression flanges." *Thin-Walled Structures*; 54:106-112.

NAS. AISI S100. (2012). *North American specification for the design of cold-formed steel structural members*. AISI S100-12, American Iron and Steel Institute, Washington, D.C..

Young B, Hancock GJ. (2003). "Compression tests of channels with inclined simple edge stiffeners." *Journal of Structural Engineering-ASCE*; 129(10):1403-1411.

Young B, Yan JT. (2004). "Design of cold-formed steel channel columns with complex edge stiffeners by Direct Strength Method." *Journal of Structural Engineering*; 30(11):1756–63.

Young B. (2005). “Experimental investigation of cold-formed steel lipped angle concentrically loaded compression members.” *Journal of Structural Engineering-ASCE*; 131(9):1390-1396.

Young B, Chen J. (2008a). “Column tests of cold-formed steel non-symmetric lipped angle sections.” *Journal of Constructional Steel Research*; 64(7-8):808-815.

Young B, Chen J. (2008b). “Design of cold-formed steel built-up closed sections with intermediate stiffeners.” *Journal of Structural Engineering*; 134(5):727-737.

Zhang JH, Young B. (2012). “Compression tests of cold-formed steel I-shaped open sections with edge and web stiffeners.” *Thin-Walled Structures*; 52:1-11.

Zhang YC, Wang CG, Zhang ZN. (2007). “Tests and finite element analysis of pin-ended channel columns with inclined simple edge stiffeners.” *Journal of Constructional Steel Research*; 63(3):383-395.

Appendix. – Notation

b_f = width of flange
b_l = depth of lip
E = initial Young's modulus
f_y = yield stress
h_w = overall depth of web
M_{EXP} = moment capacities obtained from experimental investigation
$M_{EXP\text{-}3p}$ = ultimate moments of test specimens subjected to three-point bending
$M_{EXP\text{-}4p}$ = ultimate moments of test specimens subjected to four-point bending
M_{FEA} = moment capacities obtained from finite element analysis
r_i = inner radius of the round corner of sections
t = thickness of steel plate with coating
t^* = base metal thickness
w_1, w_2, w_3 = width of plate elements of stiffened channel sections
ε = engineering strain
ε_f = strain at fracture in material coupon tests
ε_{pl} = plastic strain
θ = angle of inclined web element from the vertical axis
σ = engineering stress
$\sigma_{0.2}$ = 0.2% proof stress (yield stress)
σ_{true} = true stress
σ_u = tensile ultimate strength in material coupon tests